Role of Wood anomalies in optical properties of thin metallic films with a bidimensional array of subwavelength holes

Michaël Sarrazin,[1] Jean-Pol Vigneron,[1] and Jean-Marie Vigoureux[2]
[1]*Laboratoire de Physique du Solide, Facultés Universitaires Notre-Dame de la Paix, Rue de Bruxelles 61, B-5000 Namur, Belgium*
[2]*Laboratoire de Physique Moléculaire, UMR-CNRS 6624, Université de Franche-Comté, F-25030 Besançon Cedex, France*
(Received 16 July 2002; published 28 February 2003)

Recents works dealt with the optical transmission on arrays of subwavelength holes in a metallic layer deposited on a dielectric substrate. Making the system as realistic as possible, we perform simulations to enlighten the experimental data. This paper proposes an investigation of the optical properties related to the transmission of such devices. Numerical simulations give theoretical results in good agreement with experiment, and we observe that the transmission and reflection behavior correspond to Fano's profile correlated with resonant response of the eigen modes coupled with nonhomogeneous diffraction orders. We thus conclude that the transmission properties observed could conceivably be explained as resulting from resonant Wood's anomalies.

DOI: 10.1103/PhysRevB.67.085415 PACS number(s): 78.20.−e, 42.79.Dj, 42.25.Bs

I. INTRODUCTION

Recent papers dealt with optical experiments and simulations with various metallic gratings constituted of a thin metallic layer deposited on a dielectric substrate.[1–18] Such materials are typically one- or two-dimensional photonic crystals with a finite spatial extension in the direction perpendicular to the plane where the permittivity is periodic.

One-dimensional gratings have been widely studied, in particular on account of interesting effects knows as Wood's anomalies.[19–30] As shown by Hessel and Oliner,[19] this effect take two distinct forms. One occurs in diffraction gratings at Rayleigh wavelengths if a diffracted order becomes tangent to the plane of the grating. The diffracted beam intensity increases just before the diffracted order vanishes. The other is related to a resonance effect.[19] Such resonances come from a coupling between nonhomogeneous diffraction orders and the eigenmodes of the grating. Both types of anomalies may occur separately and independently, or appear together. Nevière and co-workers[20,21] presented a wide study of the causes of Wood's anomalies. In addition to Rayleigh wavelengths they discovered two other possible origins of such anomalies. One, called ''plasmon anomalies,'' occurs when the surface plasmons of a metallic grating are excited. The other appears when a dielectric coating is deposited on a metallic grating, and corresponds to guided modes resonances in the dielectric layer. In fact, both anomalies correspond to differents cases of the resonance effect report by Hessel and Oliner.[19] As shown by Hessel and Oliner,[19] depending on the type of periodic structure, the two kinds of anomalies (i.e., Rayleigh anomalies or resonant anomalies) may occur separately or are almost superimposed. Finally, we note that these concepts were first suggested by Fano.[22]

In this paper we perform simulations to examine the behavior of the optical properties of a device which consists of arrays of subwavelength cylindrical holes in a chromium layer deposited on a quartz substrate (Fig. 1). The values of permittivity are those obtained from experiments.[31] We present the key role of the Rayleigh wavelength and eigenmode resonances in the behavior of the zeroth order reflexion and the transmission.

Our numerical study rests on the following method. Taking into account the periodicity of the device, the permittivity is first described by a Fourier series. Then the electromagnetic field is described by Bloch waves which can also be described by a Fourier series. In this context, Maxwell equations take the form of a matricial first-order differential equation along to the *z* axis, perpendicular to the *x* and *y* axes where the permittivity is periodic.[32,33] The heart of the method is to solve this equation. One approach deals with the propagation of the solution step by step by using the scattering matrix formalism. More explicitly, we numerically divide the grating along to the *z* axis into many thick layers for which we calculate the scattering matrix. The whole scattering matrix of the system is obtained by using a special combination law applied step by step to each *S* matrix along to the *z* axis. Indeed, it is well know that S matrices and their combinations are much better conditioned than transfer

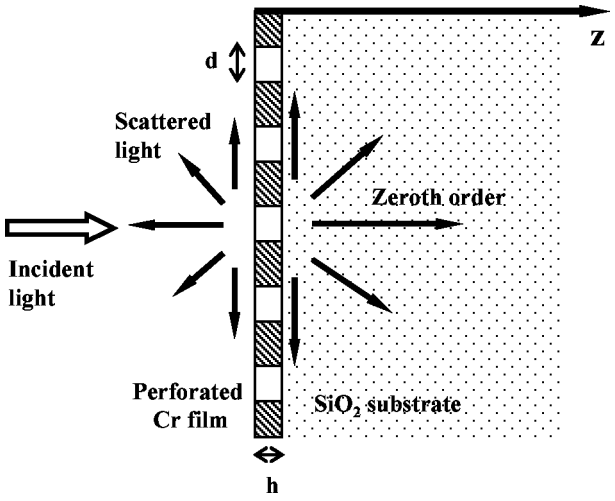

FIG. 1. Diagrammatic view of the system under study. Transmission and reflection are calculated for the zeroth order and at normal incidence as in experiments.

matrices.[33] Note that our algorithm has been compared with accuracy with others method such as Finite Difference Time Domain (FDTD) or Korringa-Kohn-Rostoker (KKR).[34] In the present work the convergence is obtained from two harmonics only, i.e., for 25 vectors of the reciprocal lattice. Furthermore, here there is no convergence problem associated with discontinuities such that we need to use Li's method.[35,36]

In the following, for a square grating of parameter a, note that, $\vec{g}=(2\pi/a)(i\vec{e}_x+j\vec{e}_y)$, such that the couple of integers (i,j) denotes the corresponding vector of the reciprocal lattice, i.e., diffraction order. Reflected and transmitted amplitudes are linked to the incident field by the use of the S scattering matrix which is calculated by solving Maxwell's equation using a Fourier series.[32] Let us define F_{scat} as the scattered field, and F_{in} as the incident field, such that

$$F_{scat}=\begin{bmatrix}\overline{N_d^+}\\ \overline{X_d^+}\\ \overline{N_v^-}\\ \overline{X_v^-}\end{bmatrix},\quad F_{in}=\begin{bmatrix}\overline{N_v^+}\\ \overline{X_v^+}\\ \overline{N_d^-}\\ \overline{X_d^-}\end{bmatrix}, \tag{1}$$

where $\overline{A}$ is a vector containing all the component $A_{\vec{g}}$. The subscripts v and d are written for the ''vacuum'' and ''dielectric substrate,'' respectively, and the superscripts $+$ and $-$ denote the positive and negative directions along the z axis for the field propagation. For each vector $\vec{g}$ of the reciprocal lattice, $N_{v\vec{g}}^-$ and $X_{v\vec{g}}^-$ are the s and p amplitudes of the reflected field, respectively, and $N_{d\vec{g}}^+$ and $X_{d\vec{g}}^+$, that of the transmitted field in the device. In the same way, $N_{v\vec{0}}^+$ and $X_{v\vec{0}}^+$ define the s and p polarization amplitudes of the incident field, respectively. Then F_{scat} is connected to F_{in} via the scattering matrix as

$$S(\lambda)F_{in}(\lambda)=F_{scat}(\lambda). \tag{2}$$

Then, the flux J of the Poynting vector through a unit cell area σ, for a incident homogeneous plane wave, is given by

$$J_v^+=\frac{\sigma}{2\mu_0\omega}k_{v\vec{0}z}[|N_{v\vec{0}}^+|^2+|X_{v\vec{0}}^+|^2], \tag{3}$$

$$J_d^+=\frac{\sigma}{2\mu_0\omega}\sum_{\vec{g}}k_{d\vec{g}z}[|N_{d\vec{g}}^+|^2+|X_{d\vec{g}}^+|^2]\times\Theta\left(\varepsilon_d(\omega)\frac{\omega^2}{c^2}-|\vec{k}_{//}+\vec{g}|^2\right), \tag{4}$$

$$J_v^-=-\frac{\sigma}{2\mu_0\omega}\sum_{\vec{g}}k_{v\vec{g}z}[|N_{v\vec{g}}^-|^2+|X_{v\vec{g}}^-|^2]\Theta\left(\frac{\omega^2}{c^2}-|\vec{k}_{//}+\vec{g}|^2\right), \tag{5}$$

where the electromagnetic field has been written as a Fourier series.[32] $\Theta(x)$ is the Heaviside function, which gives 0 for $x<0$ and $+1$ for $x>0$. $\vec{k}_{//}$ and ω are the wave vector component parallel to the surface, and the pulsation of an incident plane wave on the system, respectively. We also define

$$k_{u,\vec{g},z}=\left[\varepsilon_u\left(\frac{\omega}{c}\right)^2-|\vec{k}_{//}+\vec{g}|^2\right]^{1/2}, \tag{6}$$

where ε_u represents either the permittivity of the vacuum (ε_v), or of the dielectric substrate (ε_d). We note that if $k_{u,\vec{g},z}$ becomes imaginary then the diffraction orders become nonhomogeneous. The wavelength $(\lambda=2\pi c/\omega)$ values, such as $k_{u,\vec{g},z}=0$, are called Rayleigh wavelengths.

We define the zeroth-order transmission and reflection as

$$T_{(0)}=\frac{\sigma}{2\mu_0\omega J_v^+}k_{d\vec{0}z}[|N_{d,\vec{0}}^+|^2+|X_{d,\vec{0}}^+|^2] \tag{7}$$

and

$$R_{(0)}=-\frac{\sigma}{2\mu_0\omega J_v^+}k_{v\vec{0}z}[|N_{v\vec{0}}^-|^2+|X_{v\vec{0}}^-|^2]. \tag{8}$$

Moreover, a numerical computation of the poles of $S(\lambda)$ is important in order to study the eigenmodes of the structure. Let us write Eq. (2) as

$$S^{-1}(\lambda)F_{scat}(\lambda)=F_{in}(\lambda). \tag{9}$$

In this way, the eingenmodes of the structure are solution of Eq. (9) in the case $F_{in}(\lambda)=0$, i.e.,

$$S^{-1}(\lambda)F_{scat}(\lambda)=0. \tag{10}$$

This is a typical homogeneous problem, well known in the theory of gratings.[20,21,37–39] Complex wavelengths $\lambda_\eta=\lambda_\eta^R+i\lambda_\eta^I$, for which Eq. (10) has nontrivial solutions, are the poles of $\det[S(\lambda)]$, as we have

$$\det[S^{-1}(\lambda_\eta)]=0. \tag{11}$$

In this way, if we extract the singular part of S corresponding to the eigenmodes of the structure, we can write S in an analytical form as[20,21,37–39]

$$S(\lambda)=\sum_\eta\frac{R_\eta}{\lambda-\lambda_\eta}+S_h(\lambda). \tag{12}$$

This is a generalized Laurent series, where R_η are the residues associated with each pole λ_η. $S_h(\lambda)$ is the holomorphic part of S which corresponds to purely nonresonant processes.

Thus, assuming that $f(\lambda)$ is the mth component of $F_{scatt}(\lambda)$, we have, for the expression of $f(\lambda)$ in the neighboorhood of one pole λ_η,[20,21,37,38]

$$f(\lambda)=\frac{r_\eta}{\lambda-\lambda_\eta}+s(\lambda), \tag{13}$$

where $r_\eta=[R_\eta F_{in}]_m$ and $s(\lambda)=[S_h(\lambda)F_{in}]_m$.

II. RESULTS

The calculated transmission against the wavelength of the incident wave on the surface is shown in Fig. 2 for the zeroth diffraction order, for light incidence normal to the surface and an electric field polarized parallel to the x axis. The diameter of the holes ($d=500$ nm) and the thickness of the

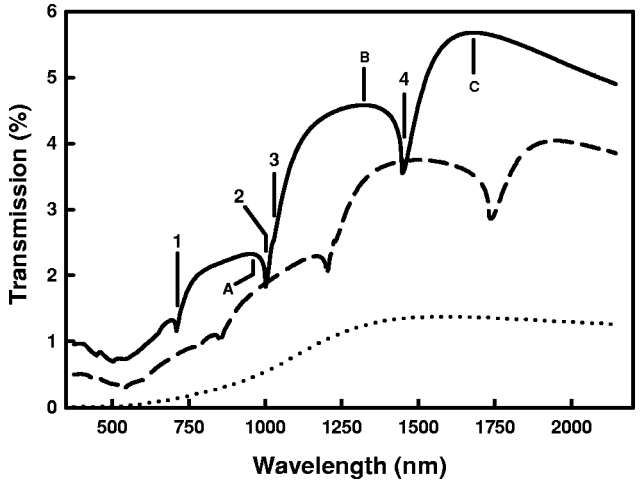

FIG. 2. Percentage transmission of the incident wave against its wavelength on the surface, for the zeroth diffraction order. The solid line denotes the transmission for the square grating of parameter $a=1$ μm, the dashed line denotes the transmission for the square grating of parameter $a=1.2$ μm, and the dotted line denotes the transmission of a similar system without holes. The points numbered 1–4 denote sudden changes in the transmission whereas the points A–C denote the maxima.

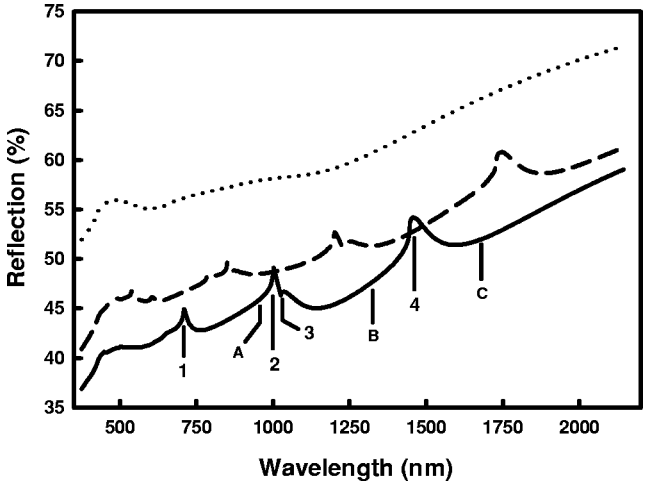

FIG. 3. Reflection against the wavelength of the incident wave on the surface, for the zeroth diffraction order. The solid line denotes the reflection for the square grating of parameter $a=1$ μm, the dashed line denotes the reflection for the square grating of parameter $a=1$, 2 μm, and the dotted line denotes the reflection of a similar system without holes. We note that the minima in Fig. 2 are matched by peaks in the reflection (see Fig. 2), numbered 1–4. We have reported the points A–C which denote the positions of maxima of the transmission.

film ($h=100$ nm) have been chosen according to the experimental conditions.[1,2] The solid and dashed lines represent the transmission for a square grating of parameters $a=1$ and 1.2 μm, respectively, whereas the dotted line corresponds to the transmission for a similar system without holes. In Fig. 2, it is shown that the transmission increases with the wavelength, and that it is characterized by sudden changes in the transmission marked 1–4 in the figure. If wavelengths 1, 2, and 4 correspond to minima, wavelength 3 is nevertheless not explicitely a minimum, as we will explain it below. These values are shifted toward larger wavelengths when the grating size increases, and the minima disappear when considering a system without a hole. Note that these results qualitatively agree with the experimental data of Ebbesen and co-workers.[1,2] Values of the wavelength marked 1–4 are given in the first column of Table I. In the second column we give the values of the positions of maxima marked A–C in the figure.

In Fig. 3 we give the calculated reflection as a function of the wavelength of the incident wave on the surface for the zeroth diffraction order, for both gratings and for a system without holes. The reflection curves are characterized by maxima (numbered 1–4) which correspond to the minima calculated in the transmission curves. In the same way, the location of these maxima are shifted toward larger wavelengths when the grating size increases, and they disappear when the surface is uniform. Then it appears that the sudden decrease in transmission is correlated with an increased reflection. Moreover, the positions of the correlated maxima and minima are calculated at wavelengths which seem to correspond to Rayleigh wavelengths, as shown in the first column of Table II. We report the positions of the maxima of transmission, marked A–C, in Fig. 3. We note that the maxima in transmission are not correlated with specifics values of the reflection.

TABLE I. Positions of minima and maxima of transmission.

Minima (nm)	Maxima (nm)
(1) 708.90	(A) 951.21
(2) 1001.44	(B) 1320.57
(4) 1447.64	(C) 1678.12

In Fig. 4 we give the calculated absorption against the wavelength of the incident wave on the surface, for the zeroth diffraction order. The solid line denotes the absorption for the square grating of parameter $a=1$ μm, the dashed line denotes the absorption for the square grating of parameter $a=1$, 2 μm, and the dotted line denotes the absorption of a similar system without holes. We report the positions of minima in Fig. 2, numbered 1–4, and the positions of points A–C which denote the maxima. These peaks are found at longer wavelengths when the grating size increases, and they disappear when the surface is uniform. Thus it appears that the sudden decrease in the transmission is caused by a combination of the increased reflection and increased loss due to surface roughness.

Previous works[1–18] identified the convex regions in the transmittance, i.e., those regions between the local minima, as regions where plasmons exist. If this were indeed the case, then we would expect to observe local maxima in the loss of energy. However, if we compare Figs. 2 and 4, we see that the convex regions in Fig. 2 are not matched by an increased loss in Fig. 4; nevertheless the maxima of absorption seems to correspond to the minima of transmission.

On the basis of these results, we investigate the role of

TABLE II. Comparison between Rayleigh wavelengths (second column) of some diffraction orders (first column) with the poles of the scattering matrix computed numerically (third column) and evaluated by measuring the wavelength of resonance λ_r, and the width Γ of some resonance curves (fourth column). (v/m) and (s/m) denote the vacuum/metal interface and substrate/metal interface, respectively.

Diffraction order	Rayleigh's wavelength (nm)	Poles (nm)	Extrapolated poles (nm)
(1,1) v/m	707.1	717.75+i20	711.88+i19.21
(1,0) v/m	1000	1010+i27	1013.26+i25.12
(1,1) s/m	1025.37	1010.25+i59	1042.81+i56.14
(1,0) s/m	1445.29	1438.75+i54	1462.41+i71

Wood's anomalies in the physical interpretation of our simulations. In this way, we emphazise the existence of eigenmodes and their role via resonant coupling with the electromagnetic field.

First we study the poles and resonances of the grating. As explained in Sec. I the existence of eigenmodes is linked to the existence of poles of the scattering matrix. If we make the assumption that the role of purely non-resonant process is negligible, i.e. $s(\lambda)\sim 0$, then Eq. (13) can be approximated by the following expression[20,21,37,38] in the vicinity of one pole $\lambda_\eta^R + i\lambda_\eta^I$:

$$|F_{scat}(\lambda)| \sim \frac{|r_\eta|}{\sqrt{(\lambda-\lambda_\eta^R)^2+\lambda_\eta^{I2}}}, \tag{14}$$

which gives a typical resonance curve where the wavelength of resonance λ_r is equal to λ_η^R, and where the width Γ at

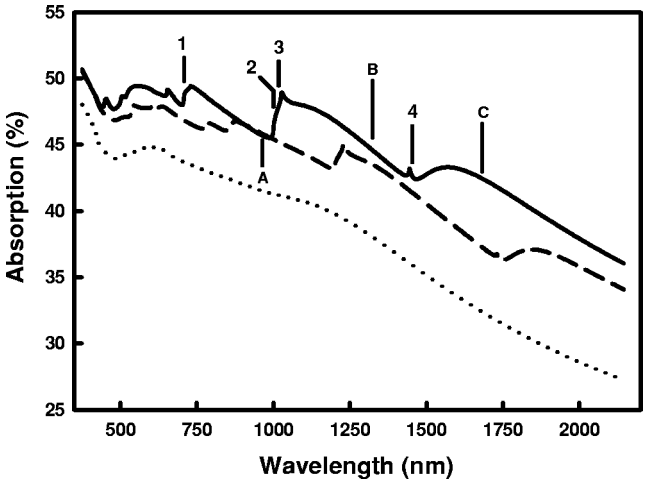

FIG. 4. Absorption against the wavelength of the incident wave on the surface, for the zeroth diffraction order. The solid line denotes the absorption for the square grating of parameter $a=1$ μm, the dashed line denotes the absorption for the square grating of parameter $a=1$, 2 μm, and the dotted line denotes the absorption of a similar system without holes. We have reported the positions of minima in Fig. 2, numbered 1–4, and the positions of points A–C which denote the maxima.

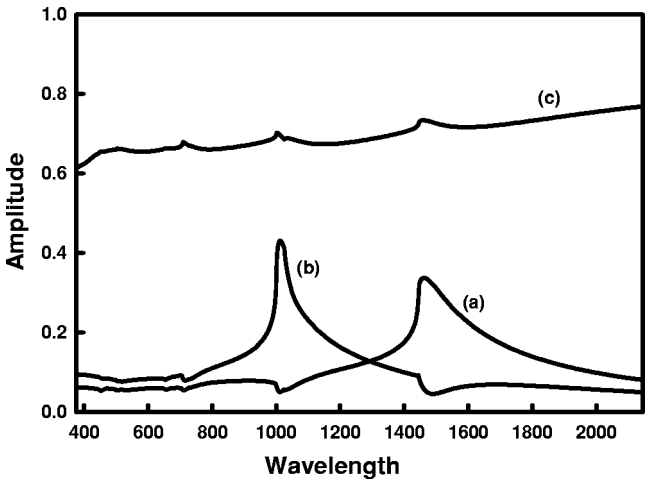

FIG. 5. Curve (a) shows the modulus of the electromagnetic field of the orders $(\pm 1,0)$ at the substrate/metal interface, as a function of the wavelength. The same holds for curve (b) but for the vacuum/metal interface. Curve (c) shows the reflected $(0,0)$ order. One notices the presence of localized peaks in curves (a) and (b). The amplitude of the incident field is equal to 1 V m^{-1}.

$(1/\sqrt{2})|F_{scat}(\lambda_r)|$ is equal to $2\lambda_\eta^I$. Before searching for a typical resonance in the behavior of diffraction orders, we check the existence of poles of the S matrix.

In the third column of Table II, we give the poles $\lambda_\eta = \lambda_\eta^R + i\lambda_\eta^I$ of the S matrix computed numerically. We keep only values whose real parts an close to values (1)–(4) in Figs. 2 and 3. This result suggests the possibility of resonant processes. In order to investigate such an assumption, we have studied the behavior of the intensity of some specific diffraction orders on the vacuum/metal and substrate/metal interfaces. More precisely, we have considered diffraction orders corresponding to the Rayleigh wavelengths connected to the positions of the minima obtained in the transmission curves. We compare the results with the transmission and reflection curves.

In Fig. 5, curve (a) shows the modulus of the electromagnetic field of the orders $(\pm 1,0)$ at the substrate/metal interface, as a function of the wavelength. The same is true for curve (b) but the interface is now vacuum/metal. Curve (c) shows the reflected $(0,0)$ order. One notices the presence of localized peaks in curves (a) and (b). Simulations allow one to check that orders $(\pm 1,0)$ have only p polarization. These peaks coincide with the minima of the curve of transmission of Fig. 2. Since these peaks correspond to orders with p polarization, they are probably resonances of the structure. To confirm this, we evaluate the poles by measuring the wavelength of resonance λ_r (which is equal to λ_η^R), and the width Γ at $(1/\sqrt{2})|F_{scat}(\lambda_r)|$ (which is equal to $2\lambda_\eta^I$). We obtain results given in the fourth column of Table II. One can easilly compare these results with those of the third column of Table II. This confirms the resonant characteristic of the diffraction orders $(\pm 1,0)$ at the metal/vacuum and metal/substrate interfaces [Hessel and Oliner called such diffraction orders ''resonant diffraction orders'' (Ref. 19)]. Note that the orders $(\pm 1,0)$ at the vacuum/metal interface and $(\pm 1,\pm 1)$ at the substrate/metal interface have poles with

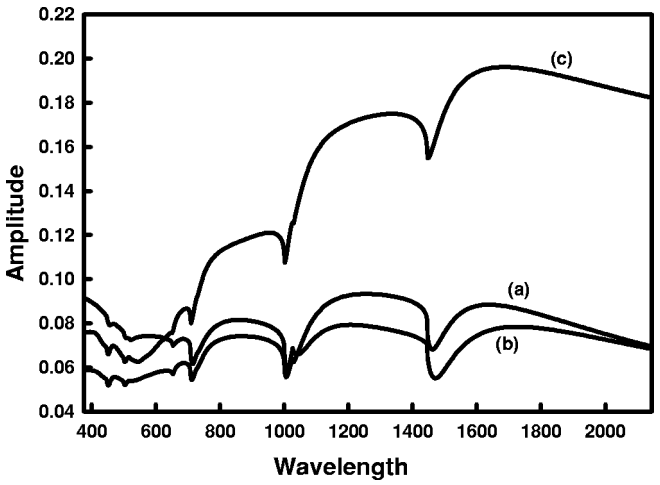

FIG. 6. Behavior of the amplitude modulus of the diffraction orders $(0,\pm 1)$, respectively for the interface vacuum/metal [curve (a)] and for the interface substrate/metal [curve (b)] as a function of the wavelength. Curve (c) corresponds to the order (0,0) in transmission. All these orders exist only with a polarization *s*. The amplitude of the incident field is equal to 1 $\mathrm{V\,m^{-1}}$.

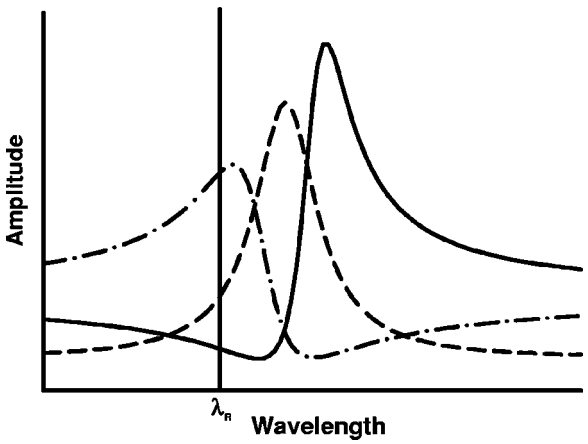

FIG. 7. Some examples of typical Fano profiles.

closer real parts. This means that both modes are almost degenerated, with the consequence that both mode effects cannot be clearly distinguished particularly for the transmission. So wavelength (3) does not seem to provide a minimum as clearly as wavelength (2).

Figure 6 shows the behavior of the amplitude modulus of the diffraction orders $(0,\pm 1)$ for the vacuum/metal [curve (a)] and for the substrate/metal [curve (b)] interfaces, respectively, as a function of the wavelength. Curve (c) corresponds to the order (0,0) in the transmission. All these orders exist only with a polarization *s*. One notices that the minima of these curves are correlated with the peaks of resonances. On the other hand, we know that orders with *s* polarization cannot present resonances. From this point of view, the minima of the curve of transmission of Fig. 2 are correlated with the resonances, while the behavior of the convex parts of the curves of transmission can be interpreted according to the profile of the orders of polarization *p*.

Let us now turn to Wood's anomalies. We consider the case where purely nonresonant process cannot be totally neglected, so that we suppose $s(\lambda)\sim s_0$. Thus it is easy to show that Eq. (13) can be written as[19,22]

$$|F_{scat}(\lambda)|^2=\frac{(\lambda-\lambda_z^R)^2+\lambda_z^{I2}}{(\lambda-\lambda_\eta^R)^2+\lambda_\eta^{I2}}|s_0|^2, \tag{15}$$

with

$$\lambda_z^R=\lambda_\eta^R-\nu^R \quad \text{and} \quad \lambda_z^I=\lambda_\eta^I-\nu^I, \tag{16}$$

where

$$\nu=\frac{r_\eta}{s}. \tag{17}$$

Coefficient ν shows the significance of resonant effects compared with purely nonresonant effects. $\lambda_z=\lambda_z^R+i\lambda_z^I$ corresponds to the zero of Eqs. (13) and (15). Equation (15) corresponds to the profiles of Fig. 7. This last expression takes into account the interferences between resonant and purely nonresonant processes. In this way, the profiles which correspond to Eq. (14), i.e., a purely resonant process, tend to become asymmetric. As shown in Fig. 7, the dashed curve shows a typically resonant process like those described by Eq. (14). On the other hand, solid and dash-dotted curves show a typical behavior where a minimum is followed by a maximum, and vice versa assuming the values of ν. These profiles tend toward $|s_0|^2$ when λ tends to $\pm\infty$. We note that these properties, which result from the interference of resonant and nonresonant processes, are similar to those described by Hessel and Oliner[19] and Fano.[22] For this reason profiles like those described in Fig. 7 are often called ''Fano profiles.''

In order to refine the interpretation of our results, in Fig. 8 we represent the three curves (transmission, reflection, and resonant diffraction order) on a more restricted domain of wavelength in the range 1300–1900 nm. In this range, since the Rayleigh wavelength is associated to the resonant diffraction order (1,0) for the metal/substrate interface, we represent the amplitude of this order only. The solid line denotes the transmission, the dashed line denotes the reflection, and the dash-dotted line denotes the amplitude of the resonant diffraction order. We also indicate the position of the corresponding Rayleigh wavelength, as well as that of the maximum of resonance (vertical dotted lines). One labels (a) the maximum of the transmission, (b) the minimum of the reflection, and (c) the maximum of the reflection.

One notices that the maximum of the resonance does not strictly coincide with the maximum of the reflection and the minimum of the transmission. Also, one notices that the maximum of the reflection does not coincides with the minimum of the transmission. On the other hand, the Rayleigh wavelength seems to correspond well with the minimum of the transmission. We notice that the diffraction order is homogeneous for wavelengths lower than the Rayleigh wavelength. For this reason, the resonance peak cannot be observed for wavelengths lower than Rayleigh wavelengths. So, if one intends to take away the position of the resonance of the value of the Rayleigh wavelength, one can make it *a*

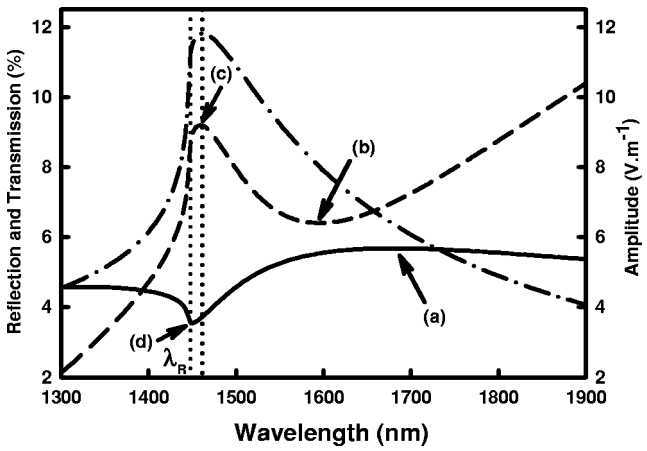

FIG. 8. The set of three curves (transmission, reflection and resonant diffraction order) on a more restricted domain of wavelength included between 1300 and 1900 nm. In this domain Rayleigh's wavelength is associated with the diffraction order (1,0) of the interface metal/substrate. We also indicate the position of the wavelength of the corresponding Rayleigh wave as well as that of the maximum of resonance. (*a*) is the maximum of the transmission, (*b*) the minimum of the reflection, and (*c*) the maximum of the reflection. Solid line: transmission; dashed line: reflection; dash-dotted line: resonant diffraction order. The amplitude of the incident field is equal to 1 V m^{-1}.

priori only in the direction of increasing wavelengths. Should the opposite occur, the position of the resonance peak tends toward Rayleigh's value.

As in Fig. 8, in Fig. 9 we represent the three curves (transmission, reflection, and resonant diffraction order) for the same physical parameters. However, whereas in the previous case the value of the permittivity of the metal film was that of chromium,[31] we now use a value equal to $-25+i1$ which does not depend on the wavelength. Such a value of the permittivity does not correspond to an existing material. We

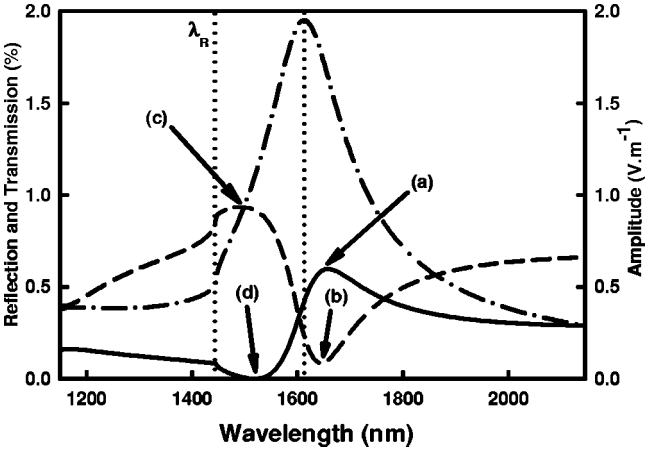

FIG. 9. A similar system to that in Fig. 8 except that the value of the permittivity of the metal film here is equal to $-25+i1$. As in Fig. 8, (*a*) is the maximum of the transmission, (*b*) the minimum of the reflection, and (*c*) the maximum of the reflection. (*d*) is the minimum of the transmission. The amplitude of the incident field is equal to 1 V m^{-1}.

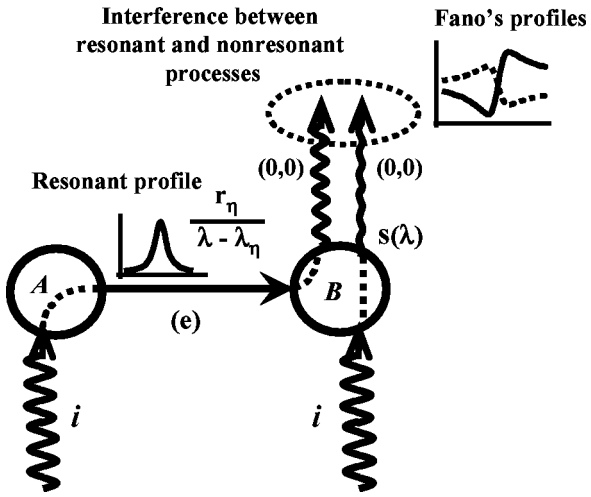

FIG. 10. Diagrammatic representation of the processes responsible for the behavior of the transmission properties.

choose this permittivity value for the metal such that we select a peak of resonance farther from the Rayleigh wavelength than in the previous case. The choice of this value comes from research on the compromise between the position of the peak of resonance and its width, so as to illustrate our matter clearly. As in Fig. 8, (*a*) is the maximum of the transmission, (*b*) the minimum of the reflection, and (*c*) the maximum of the reflection. (*d*) is the minimum of the transmission.

This time, one notices in a clear way the absence of coincidence between the peak of the resonance and the minima (respectively the maxima) of the reflection (respectively of transmission). Contrary to what is generally assumed,[1–16] one sees that the nonresonant Wood's anomalies connected to Rayleigh wavelengths are not the cause of the minima of the transmission. They simply correspond to a discontinuity of each of the three curves. It is particularly important to note that the profiles of the transmission and reflection correspond to Fano profiles, as discussed below. One can interpret the behavior of these spectra in terms of resonant Wood's anomalies in the sense described by Fano[22] and by Hessel and Oliner.[19]

III. DISCUSSION

In order to understand the physical mechanisms responsible for the behavior observed in Figs. 8 and 9, in Fig. 10 we represent the corresponding involved processes. In Fig. 10, circles *A* and *B* represent diffracting elements (e.g., holes). So an incident homogeneous wave (*i*) diffracts in *A* and generates a nonhomogeneous resonant diffraction order (*e*) [e.g. (1,0)]. Such an order is coupled with an eigenmode which is characterized by a complex wavelength λ_η. It becomes possible to excite this eigenmode, which leads to a feedback reaction on the order (e). This process is related to the resonant term.

The diffraction order (*e*) diffracts in *B*, and generates a contribution to the homogenous zero diffraction order $(0,0)$. Thus one can ideally expect to observe a resonant profile,

i.e., Lorentzian-like, for the homogenous zero diffraction order (0,0) which appears in *B*. Nevertheless, it is necessary to account for nonresonant diffraction processes related to the holomorphic term. So incident wave (i), here represented in *B*, generates a homogeneous zero order. Then one takes into account the interference of two rates, resonant and nonresonant contributions to zero order. The resulting line shapes are typically Fano profiles which correspond to resonant processes where one takes nonresonant effects into account. One notes that a maximum in the transmission does not necessary correspond to a maximum of the resonance of a diffraction order. This is exactly the process observed in Fig. 9, where the resonance is associated with the diffraction order (1,0). So, the Fano profiles of the reflection and transmission result from a superimposition of resonant and nonresonant contributions to the zero diffraction order.

If one refers to Fig. 8, the concrete case of chromium, the resonance is closer to the Rayleigh wavelength than in the case of Fig. 9. On the other hand, the positions of the maximum and minimum of a Fano profile are determined by the resonance position. More precisely, if the resonance is shifted in a given direction, the maximum and minimum of the Fano profile tend to be shifted in the same way. Consequently, in the present case, the maximum and minimum of the asymmetric Fano's profile are shifted toward the Rayleigh wavelength in the same way as the resonant response. In Fig. 8, in the case of the transmission, minimum (*d*) is not of the same kind of the minimum (*d*) in Fig. 9. This is not a true minima of the Fano profile. All occurs as if the minimum of the Fano profile disappears behind the Rayleigh wavelength toward low wavelength. In other words, the minimum (*d*) in Fig. 8 comes from the cutoff and the discontinuity introduced between the minimum and the maximum of the Fano profile at the Rayleigh wavelength. On the other hand, note that maximum (*a*) of the transmission and maximum (*c*) of the reflection just localized rests after the Rayleigh wavelength. For the reflection, minima (*b*) tend to be shifted toward a low wavelength.

Previous works[1–16] identified the convex regions in transmission, i.e., the regions between the minima, as regions where plasmons exist. The present study tends to qualify this hypothesis, since it shows that the experimental results can be described in terms of Wood's anomalies. Indeed, as shown by Fano[22] and Hessel and Oliner,[19] for one-dimesionnal gratings, Wood's anomalies can be treated in terms of eigenmodes grating excitation. In this context, these authors demonstrated the asymmetric behavior of the intensities of the homogeneous diffraction orders according to the wavelength. One can conclude that the results of Ebbesen's experiments correspond to the observation of resonant Wood's anomalies.

Here, as we use metal in our device, it seems natural to assume that these resonances are surface plasmons resonances. Nevertheless, it is important to note that our analysis does not make raise hypothesis as to the origin of the eigenmodes. This means that it could be possible to obtain transmission curves similar to those for metals, by substituting the surface plasmons by polaritons or guided modes. This work is in progress.

IV. CONCLUSION

Using a system similar to that used in recent papers,[1,2] we have shown that numerical simulations give theoretical results in good qualitative agreement with experiments. Previous authors suggested that the results are due to the presence of a metallic layer, such that the surface plasmons could give rise to transmission curves of these characteristics. We have performed simulations using the same geometry, and observed that the transmission and reflection behaviors correspond to Fano profiles correlated with the resonant response of the eigenmodes coupled with nonhomogeneous diffraction orders. We thus conclude that the transmission properties observed could conceivably be explained as resulting from resonant Wood's anomalies.

ACKNOWLEDGMENTS

We acknowledge the use of Namur Scientific Computing Facility (Namur-SCF), a common project between the FNRS, IBM Belgium, and the Facultés Universitaires Notre-Dame de la Paix (FUNDP). This work was carried out with support from EU5 Centre of Excellence ICAI-CT-2000-70029 and from the Inter-University Attraction Pole (IUAP P5/1) on ''Quantum-size effects in nanostructred materials'' of the Belgian Office for Scientific, Technical, and Cultural Affairs.

[1] T.W. Ebbesen, H.J. Lezec, H.F. Ghaemi, T. Thio, and P.A. Wolff, Nature (London) **391**, 667 (1998).
[2] T. Thio, H.F. Ghaemi, H.J. Lezec, P.A. Wolff, and T.W. Ebbesen, J. Opt. Soc. Am. B **16**, 1743 (1999).
[3] H.F. Ghaemi, T. Thio, D.E. Grupp, T.W. Ebbesen, and H.J. Lezec, Phys. Rev. B **58**, 6779 (1998).
[4] U. Schröter and D. Heitmann, Phys. Rev. B **58**, 15 419 (1998).
[5] D.E. Grupp, H.J. Lezec, T. Thio, and T.W. Ebbesen, Adv. Mater. **11**, 860 (1999).
[6] T.J. Kim, T. Thio, T.W. Ebbesen, D.E. Grupp, and H.J. Lezec, Opt. Lett. **24**, 256 (1999).
[7] J.A. Porto, F.J. Garcia-Vidal, and J.B. Pendry, Phys. Rev. Lett. **83**, 2845 (1999).
[8] Y. M. Strelniker and D. J. Bergman, Phys. Rev. B **59**, 12 763 (1999).
[9] S. Astilean, Ph. Lalanne, and M. Palamaru, Opt. Commun. **175**, 265 (2000).
[10] D.E. Grupp, H.J. Lezec, T.W. Ebbesen, K.M. Pellerin, and T. Thio, Appl. Phys. Lett. **77**, 1569 (2000).
[11] E. Popov, M. Nevière, S. Enoch, and R. Reinisch, Phys. Rev. B **62**, 16 100 (2000).
[12] W.-C. Tan, T.W. Preist, and R.J. Sambles, Phys. Rev. B **62**, 11 134 (2000).
[13] T. Thio, H.J. Lezec, and T.W. Ebbesen, Physica B **279**, 90 (2000).

[14] A. Krishnan, T. Thio, T.J. Kim, H.J. Lezec, T.W. Ebbesen, P.A. Wolff, J. Pendry, L. Martin-Moreno, and F.J. Garcia-Vidal, Opt. Commun. **200**, 1 (2001).
[15] L. Martin-Moreno, F.J. Garcia-Vidal, H.J. Lezec, K.M. Pellerin, T. Thio, J.B. Pendry, and T.W. Ebbesen, Phys. Rev. Lett. **86**, 1114 (2001).
[16] L. Salomon, F. Grillot, A.V. Zayats, and F. de Fornel, Phys. Rev. Lett. **86**, 1110 (2001).
[17] M.M.J. Treacy, Appl. Phys. Lett. **75**, 606 (1999).
[18] J.-M. Vigoureux, Opt. Commun. **198**, 257 (2001).
[19] A. Hessel and A.A. Oliner, Appl. Opt. **4**, 1275 (1965).
[20] D. Maystre and M. Nevière, J. Opt. **8**, 165 (1977).
[21] M. Nevière, D. Maystre, and P. Vincent, J. Opt. **8**, 231 (1977).
[22] V.U. Fano, Ann. Phys. (N.Y.) **32**, 393 (1938).
[23] R.H. Bjork, A.S. Karakashian, and Y.Y. Teng, Phys. Rev. B **9**, 1394 (1974).
[24] P.J. Bliek, L.C. Botten, R. Deleuil, R.C. Mc Phedran, and D. Maystre, IEEE Trans. Microwave Theory Tech. **MTT-28**, 1119 (1980).
[25] D. Deaglehole, Phys. Rev. Lett. **22**, 14, 708 (1969).
[26] E. Popov, L. Tsonev, and D. Maystre, Appl. Opt. **33**, 5214 (1994).
[27] Lord Rayleigh, Proc. R. Soc. London, Ser. A **79**, 399 (1907).
[28] K. Utagawa, J. Opt. Soc. Am. **69**, 333 (1979).
[29] L. Wendler, T. Kraft, M. Hartung, A. Berger, A. Wixforth, M. Sundaram, J.H. English, and A.C. Gossard, Phys. Rev. B **55**, 2303 (1997).
[30] R.W. Wood, Phys. Rev. **48**, 928 (1935).
[31] D.W. Lynch and W.R. Hunter, in *Handbook of Optical Constants of Solids II*, edited by E.D. Palik (Academic, New York, 1991).
[32] J.P. Vigneron, F. Forati, D. André, A. Castiaux, I. Derycke, and A. Dereux, Ultramicroscopy **61**, 21 (1995).
[33] J.B. Pendry and P.M. Bell, in *Photonic Band Gap Materials of NATO Advanced Study Institute, Series B*: Vol. 315, edited by C.M Soukoulis (Kluwer Academic, Dordrecht, 1995).
[34] V. Lousse and K. Ohtaka (private communication).
[35] L. Li, J. Opt. Soc. Am. A **13**, 1870 (1996).
[36] L. Li, J. Opt. Soc. Am. A **14**, 2758 (1997).
[37] E. Centeno and D. Felbacq, Phys. Rev. B **62**, R7683 (2000).
[38] E. Centeno and D. Felbacq, Phys. Rev. B **62**, 10 101 (2000).
[39] R. Petit, *Electromagnetic Theory of Gratings*, Topics in Current Physics, Vol. 22 (Springer-Verlag, Berlin, 1980).